ACS APPLIED MATERIALS & INTERFACES

www.acsami.org

Research Article

Optimized Molecular Packing and Nonradiative Energy Loss Based on Terpolymer Methodology Combining Two Asymmetric Segments for High-Performance Polymer Solar Cells

Xunchang Wang, Jianhua Han, Da Huang, Jianing Wang, Yuan Xie, Zhilin Liu, Yonghai Li, Chunming Yang,* Yong Zhang, Zhicai He, Xichang Bao,* and Renqiang Yang*

Cite This: *ACS Appl. Mater. Interfaces* 2020, 12, 20393−20403

Read Online

ACCESS | Metrics & More | Article Recommendations | Supporting Information

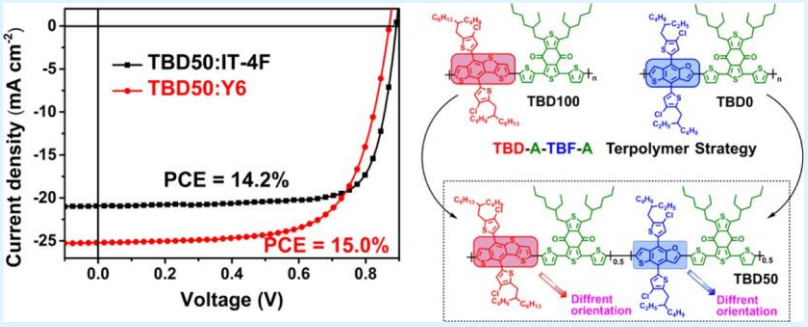

ABSTRACT: In this work, a random terpolymer methodology combining two electron-rich units, asymmetric thienobenzodithiophene (TBD) and thieno[2,3-*f*]benzofuran segments, is systematically investigated. The synergetic effect is embodied on the molecular packing and nanophase when copolymerized with 1,3-bis(2-ethylhexyl)benzo[1,2-*c*:4,5-*c*′]dithiophene-4,8-dione, producing an impressive power conversion efficiency (PCE) of 14.2% in IT-4F-based NF-PSCs, which outperformed the corresponding D−A copolymers. The balanced aggregation and better interpenetrating network of the TBD50:IT-4F blend film can lead to mixing region exciton splitting and suppress carrier recombination, along with high yields of long-lived carriers. Moreover, the broad applicability of terpolymer methodology is successfully validated in most electron-deficient systems. Especially, the TBD50/Y6-based device exhibits a high PCE of 15.0% with a small energy loss (0.52 eV) enabled by the low nonradiative energy loss (0.22 eV), which are among the best values reported for polymers without using benzodithiophene unit to date. These results demonstrate an outstanding terpolymer approach with backbone engineering to raise the hope of achieving even higher PCEs and to enrich organic photovoltaic materials reservoir.

KEYWORDS: *nonfullerene solar cell, random terpolymer, asymmetrical structure, microstructure, nonradiative energy loss, power conversion efficiency*

INTRODUCTION

As one of the potential green technologies for utilizing solar energy, solution-processed polymer solar cells (PSCs) with advantages such as tailorable structure, flexibility, lightweight, and potentially large-area fabrication have attracted considerable attention from academics and industry.[1−5] The most typical bulk-heterojunction (BHJ) PSCs consist of a p-type conjugated polymer as the donor and an n-type organic semiconductor as the acceptor.[6,7] In the past few years, benefiting from the rapid development of fused-ring electron acceptors (FREAs), which feature more extended optical absorption and facile energy level modulation than those of traditional fullerene acceptors,[8−17] the power conversion efficiency (PCE) has been dramatically improved over 17% for single junction and tandem PSCs.[18−21]

Compared with the high-performance diverse FREA materials, the development of state-of-the-art donor polymers mainly relies on the concept of the alternating donor−acceptor (D−A), which can be precisely controlled by the regularity of the polymer backbone, and only a few polymeric moieties such as benzodithiophene (BDT), 1,3-bis(2-ethylhexyl)benzo[1,2-*c*:4,5-*c*′]dithiophene-4,8-dione (BDD), difluorobenzo[1,2,3]-triazole, difluorobenzotriazole, thieno[3,4-*b*]thiophene, alkoxycarbonyl-bithiophene, and thiophene-quinoxaline units have

Received: January 24, 2020
Accepted: April 14, 2020
Published: April 14, 2020

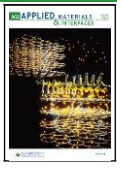

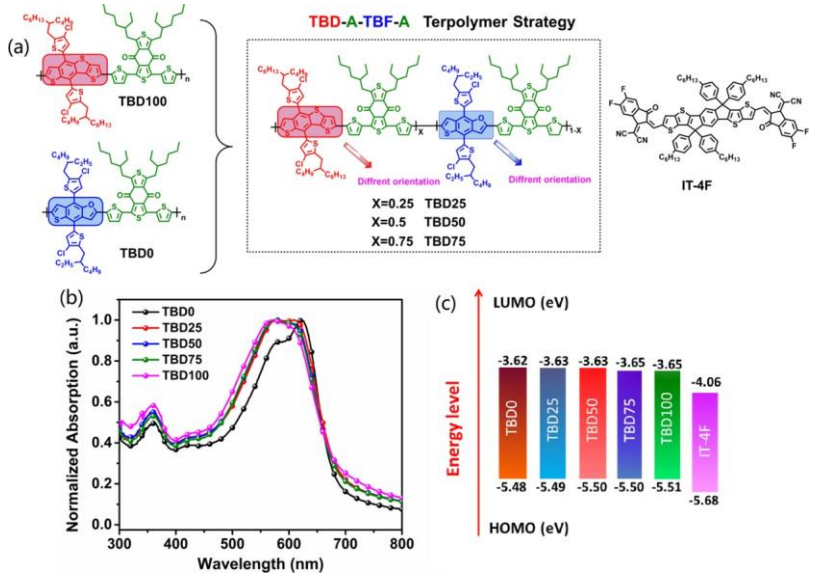

Figure 1. (a) Chemical structures of the donor polymers and IT-4F. (b) Normalized ultraviolet−visible absorption of the polymers as neat films. (c) Energy level diagram of the polymers and IT-4F in thin films.

been successfully applied to achieve a high PCE in PSCs.[11,22−33] Especially in nonfullerene (NF)-PSCs, except for a handful of structures, PTQ10,[29] PNDT-ST,[31] PHI-ffBT,[32] etc., almost all efficient polymers (PCE > 12%) are predominant by the BDT-based unit, and most of the works are focused on side-chain engineering, embedding or changing π-bridge types.[34−43] Therefore, it is of great significance and urgency to further excavate the potential of FREA materials (such as IT-4F and Y6), break the monopolization of BDT units, and develop more efficient polymer donor materials with modulated morphology and minimized energy loss to match with updated acceptors.

Random copolymerization has emerged as a promising synthetic approach involving three different components in polymer backbones, which can induce synergistic effect on optical, electrochemical, and morphological properties via fine-tuning the molar ratio of each structure.[44−52] For instance, Hou et al. introduced the ester group-substituted thiophene unit into PM6, settled in a terpolymer system by newly generated absorption, leading to a broad band gap and an improved PCE over 15%.[51] In addition, the energy loss can also be regulated by a terpolymer. For example, Yan et al. incorporated a both fluoro and ester monothiophene into polymer PM6; the synergistic effect was observed on downshifting the energy levels and lowering the energy loss in the Y6-based device, leading to a high PCE of 16.4%.[33] These results indicated that investigating the relationship between structure−properties of terpolymers should still be significant.

To broaden the available candidates for making high-performance photovoltaic materials, recently, we presented a new electron-donating moiety thienobenzodithiophene (TBD) with an asymmetric backbone,[53] and different band gaps of TBD-based polymers can be obtained by polymerization with various electron-deficient structures, matching with small-molecule acceptors or polymer acceptors. Compared with the BDT unit, construction of donor polymers with the TBD unit for PSCs can achieve improved open-circuit voltage (V_{oc}) while without sacrificing short-circuit current density (J_{sc}). Another promising electron-donating structure, thieno[2,3-*f*]benzofuran (TBF), which possesses some unique and particular features, has rarely been systematically investigated in PSCs.[54,55] The smaller atomic radius of oxygen in the furan ring with an intense electronegativity can induce stronger molecular aggregation and guarantee a more planar structure for charge transport.[56] However, the excessive aggregation of TBF-based polymers in blend films can affect large phase separation and exciton recombination and thus lower device performance. In order to alleviate the weaknesses of each structure and construct high-performance donor materials, we try to combine these two asymmetric structures in the terpolymer backbone, with an intention to stepwise modulate the intrachain and/or interchain interactions and BHJ morphology evolution and meanwhile reduce the energy loss. On the basis of the above considerations, we first utilized the random copolymerization approach by partially replacing TBD with the TBF segment in an alternating BDD and TBD copolymer. TBD*x* exhibits suitable optical absorption and energy level, matching well with the efficient acceptor IT-4F.[57] The blend morphology of active layers, charge carrier mobilities, and photovoltaic properties was found to vary substantially with the varied copolymer composition. The best efficiency of 14.2% was achieved in optimized PSCs based on the terpolymer (TBD50) containing 50 wt % TBD, which is among the highest values reported for IT-4F-based NF-PSCs. The excellent performance is mainly attributed to the synergistic effect induced by the optimized TBD−TBF ratio, balancing phase separation and crystallization and triggering high yields of long-lived charges of the device. Moreover, the broad applicability of our terpolymer strategy is successfully validated in different polymer/nonfullerene acceptor (NFA) systems, exhibiting high photovoltaic efficiencies of 13.0, 11.8, and 15.0% for R-Tz:IT-4F, R-DTBT:IT-4F, and TBD50:Y6-based devices. Notably, the TBD50:Y6-based device delivers a nonradiative energy loss of 0.22 eV, which is lower than that of the famous PM6/Y6- (0.29 eV) and PM7/Y6- (0.24 eV) based devices. Thus, our results demonstrate that the combination of asymmetric TBD and TBF segments in the terpolymer backbone can exhibit the great potential to modulate the

https://dx.doi.org/10.1021/acsami.0c01323
ACS Appl. Mater. Interfaces 2020, 12, 20393−20403

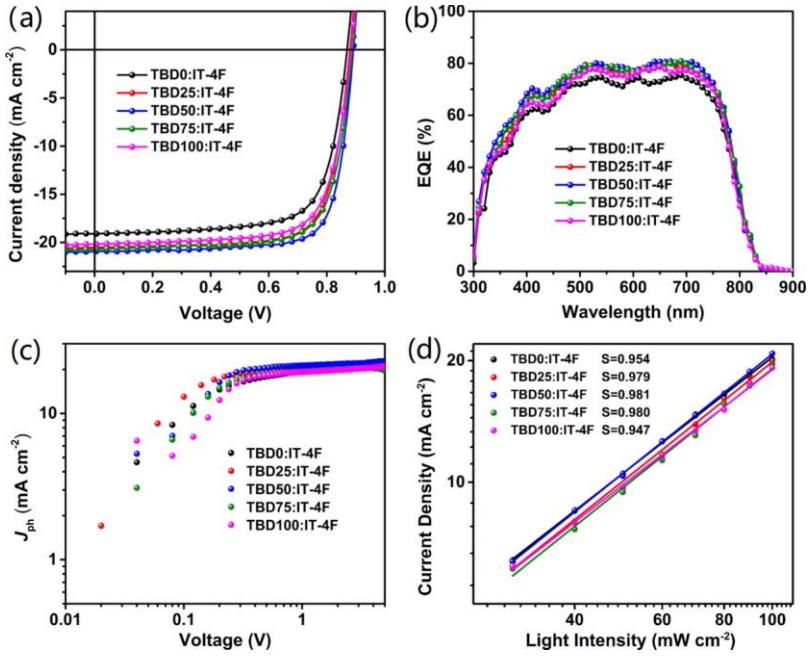

Figure 2. (a) $J-V$ characteristics of the optimized PSCs based on the polymers and IT-4F. (b) EQE curves of the corresponding PSCs. (c) J_{ph} vs V_{eff} curves of the optimized BHJ devices. (d) $J_{ph}-P_{light}$ curves of the optimized devices.

morphology and reduce nonradiative energy loss and achieve high-performance NF-PSCs.

RESULTS AND DISCUSSION

The new random polymers, TBDx (x = 0, 25, 50, 75, 100) in which the TBD and TBF linkages are randomly distributed in the backbone, were prepared using palladium-catalyzed cross-coupling condensation polymerization, as shown in Figure 1 and Scheme S1. The polymers were obtained in high yields (60−80%), and fully synthetic details are included in the Supporting Information. TBDx polymers showed excellent solubility in organic solvents (e.g., chloroform, chlorobenzene, and dichlorobenzene). Their molecular weights were estimated by high-temperature gel permeation chromatography using 1, 3, 5-trichlorobenzene as the eluent at 150 °C, and the resulting number-averaged molecular weights are in the range of 51.5−84.2 kDa with a polydispersity index of 1.96−2.46 (Figure S1 and Table S1). As shown in Figure S2, the decomposition temperature at 5% weight loss (T_d) determined from thermogravimetric analysis curves is all over 400 °C. The UV−vis absorption spectra of the polymers were measured both in solution and in thin films, as shown in Figures S3 and 1. Compared to polymer TBD0, the polymers with a proportion of asymmetric TBD units exhibit an obvious blue-shifted absorption maximum (≈10 nm) and a weak 0−0 peak, which can be attributed to the reduced planarity and stacking of polymers, weakening aggregation properties[50] (Figure S4). However, it scarcely affects the optical band gap (E^{opt}) as the five polymers have similar film absorption onsets (corresponding to the similar E_g^{opt} of 1.87 eV, Table S1). Cyclic voltammetry measurements were used to estimate the energy levels of these polymers by using the onset of oxidation potential and reduction potential. All of the terpolymers exhibited an almost similar highest occupied molecular orbital level (≈−5.50 eV), which was further confirmed by the ultraviolet photoelectron spectroscopy measurements (Figures 1c and S4).

To study the optimized molecular conformation of the terpolymers, density functional theory calculation at the B3LYP/6-31G(d,p) basis set was conducted. All the alkyl side chains were omitted to simplify the calculations. As summarized in Figure S5a,b, extremely small dihedral angles of 2.23 and 2.74° are found in the conjugated backbone of polymer TBD0, which may result from the noncovalent intramolecular O···S interactions, in contrast to those in the TBD100 backbone. Note that the asymmetric TBD segment has dual orientation; introducing this segment to polymer TBD0 can reduce the planarity of TBF-based polymers and lead to a balanced dihedral angle on each side of the TBD backbone, thus reasonably modulating the molecular interaction and aggregation. To further help understand the synergetic effect of random insertion of asymmetric TBD and TBF segments at the molecular level, grazing-incidence wide-angle X-ray scattering (GIWAXS) was examined to reveal the molecular packing and crystallinity of neat polymer films (Figure S5c,d). The pure TBD0 film shows a highly ordered structure with preferential face-on orientation, as confirmed by the pronounced (010) π−π stacking peak in the out-of-plane (OOP) direction and a strong (100) lamellar peak in the in-plane (IP) direction. With regard to the three TBD-A−TBF-A-based terpolymers, the similar diffraction features are observed. A (010) peak located at q_z = 1.76 Å^{-1} is identified, assigned to the π−π stacking distance of 3.57 Å, which is larger than that of polymer TBD0 (3.50 Å), indicating that insertion of TBD segments in TBD0 can weaken crystallinity and hinder the aggregation of the polymer, which is consistent with the blue-shifted absorption spectra of the terpolymers. Thus, the TBF segment can provide terpolymers with high ordered orientation, but the opposite properties are observed when incorporating the TBD segment, weakening the crystallinity yet maintaining the predominant face-on orientation of the terpolymers.

Single-junction PSCs with a conventional structure of ITO/PEDOT:PSS/polymer:IT-4F/PDINO/Al were fabricated to

https://dx.doi.org/10.1021/acsami.0c01323
ACS Appl. Mater. Interfaces 2020, 12, 20393−20403

Table 1. Photovoltaic Parameters of the PSCs under the Illumination of AM 1.5G, 100 mW cm^{-2}

active layer	V_{oc}[a] (V)	J_{sc}[a] (mA cm^{-2})	J^{EQE} (mA cm^{-2})	FF[a] (%)	PCE[a] (%)
TBD0:IT-4F	0.870 (0.86 ± 0.005)	19.0 (18.8 ± 0.3)	18.5	0.722 (0.708 ± 0.015)	12.0 (11.7 ± 0.3)
TBD25:IT-4F	0.880 (0.878 ± 0.004)	20.5 (20.2 ± 0.3)	19.7	0.747 (0.736 ± 0.013)	13.5 (13.3 ± 0.2)
TBD50:IT-4F	0.892 (0.890 ± 0.003)	20.8 (20.6 ± 0.3)	19.8	0.768 (0.754 ± 0.015)	14.2 (14.0 ± 0.2)
TBD75:IT-4F	0.888 (0.885 ± 0.003)	20.7 (20.5 ± 0.2)	19.8	0.740 (0.726 ± 0.016)	13.6 (13.4 ± 0.3)
TBD100:IT-4F	0.883 (0.880 ± 0.004)	20.3 (19.8 ± 0.4)	19.4	0.729 (0.714 ± 0.014)	13.00 (12.8 ± 0.2)

[a]The values in parentheses are the average values with standard deviations obtained from 15 devices. The thickness of the active layer is 110 ± 15 nm.

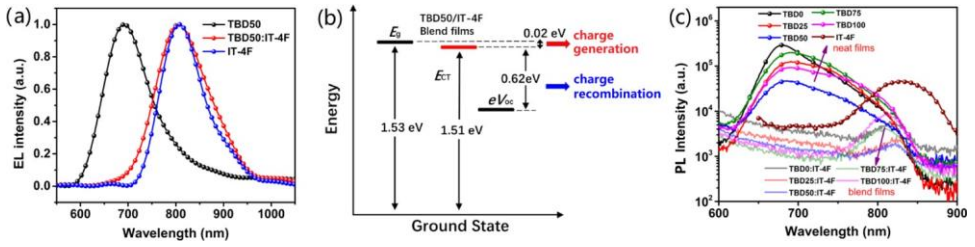

Figure 3. (a) EL spectra of the neat TBD, IT-4F, and TBD−TBF blend films. (b) Illustration of voltage loss diagram for the TBD50/IT-4F-based device. (c) PL spectra of the pure polymers and their blend films with IT-4F.

investigate the terpolymer methodology effect on the photovoltaic properties. Detailed fabrication procedures and the different optimized conditions for the devices are depicted in the Supporting Information. The current density−voltage ($J-V$) curves of the PSCs under the optimal conditions are shown in Figure 2a, and the corresponding data are summarized in Tables 1 and S2. An inferior PCE of 12.0% with low J_{sc} is recorded from the TBD0:IT-4F-based device. Upon increasing the TBD content in the main chain, especially in the TBD50/IT-4F device, the boosted PCE of 14.2% is achieved along with a high J_{sc} of 20.8 mA/cm^2 and a fill factor (FF) of 76.8%, to be one of the highest PCE values in the IT-4F system. However, the drops in FF and PCE are also observed with further increase in TBD fraction. The remarkable different morphology of the polymer owing to the variation on the TBD−TBF composition is considered to be one of the important factors responsible for the significant differences in the final photovoltaic performance. The calculated J_{sc} values obtained by integrated external quantum efficiency (EQE) spectra are in good agreement with those obtained from the $J-V$ curves (small deviation less than 5%), suggesting that the $J-V$ measurements are highly reliable (Figure 2b).

The photocurrent density (J_{ph}) versus the effective voltage (V_{eff}) was measured to investigate the charge dissociation process (Figure 2c).[58] J_{ph} is determined by J_L-J_D, where J_L and J_D are the current densities under illumination and in dark, respectively, and V_{eff} is obtained from V_0 to V_a (where V_0 is the voltage when J_{ph} = 0 and V_a is the bias voltage). The sufficiently high V_{eff} (>4 V) was utilized to obtain the saturation photocurrent density (J_{sat}). Under the short-circuit current state, the terpolymer:IT-4F-based devices showed higher exciton dissociation probability than that of the copolymer:IT-4F-based devices, which implied that more efficient charge dissociation and charge collection processes were achieved. Furthermore, this is likely due to the optimal morphology in the terpolymer blends and further gives support to the observed high J_{sc} and FF in terpolymer-based devices. To gain insights into the charge recombination of the random terpolymer-based devices, the J_{sc}s as a function of illumination intensity (P_{light}) were measured (Figure 2d), and they have a relationship of $J_{sc} \propto P_{light}^{S}$, where S is a power-law scaling exponent. When the fitting slope value S is close to 1, the bimolecular recombination in the devices can be negligible.[59] The terpolymer-based devices show a value close to 1 (≈0.980), which is higher than those of D−A copolymers such as TBD0 (0.954) and TBD100 (0.947) devices, indicating the reduced bimolecular recombination in terpolymer:IT-4F devices and accounting for their improved J_{sc} and FF.

To understand the charge transport evolution induced by combining TBD and TBF segments, we investigated the charge carrier mobilities of the TBDx:IT-4F blend films with the same condition for optimal solar cells by using space-charge-limited current measurement (Figure S6). The calculated μ_h and μ_e values are summarized in Table S3. It is found that the carrier mobilities of the terpolymer blend films are higher than that of the corresponding TBD0 and TBD100 blend films. The observed increase of hole and electron mobilities and balanced charge transport in the random terpolymer blend films could reduce bimolecular recombination in solar cells, thereby promoting charge extraction and improving J_{sc} and FF values.

Furthermore, the electroluminescence (EL) was measured to search for the position of charge transfers (CTs) of blend films, and TBD50 was selected as an example to analyze the energy loss (E_{loss}) in detail (Figures 3 and S7). The energy loss can be divided into two parts: the first part of loss from excitons (singlet state, S1) to CT states that occurred during charge generation and the second part of loss between CTs and final V_{oc} that was generated during the charge recombination process.[60−62] Compared with the neat TBD and IT-4F, the TBD50:IT-4F blend film exhibits a broad EL spectrum, which is attributed to the reorganization energy of the CT state. The maximum peak of the blend film is around 820 nm, assigned to the E_{CT} of 1.51 eV, almost approaching to the E_g of 1.53 eV of the blend film. From Figure 3b and the above analysis, the total V_{oc} loss of the TBD-based device is 0.64 eV, along with the sum of radiative and nonradiative energy loss of 0.62 eV during the charge separation and transport process. In addition, the resemblance of the CT position was found for all the five polymers, which is consistent

https://dx.doi.org/10.1021/acsami.0c01323
ACS Appl. Mater. Interfaces 2020, 12, 20393−20403

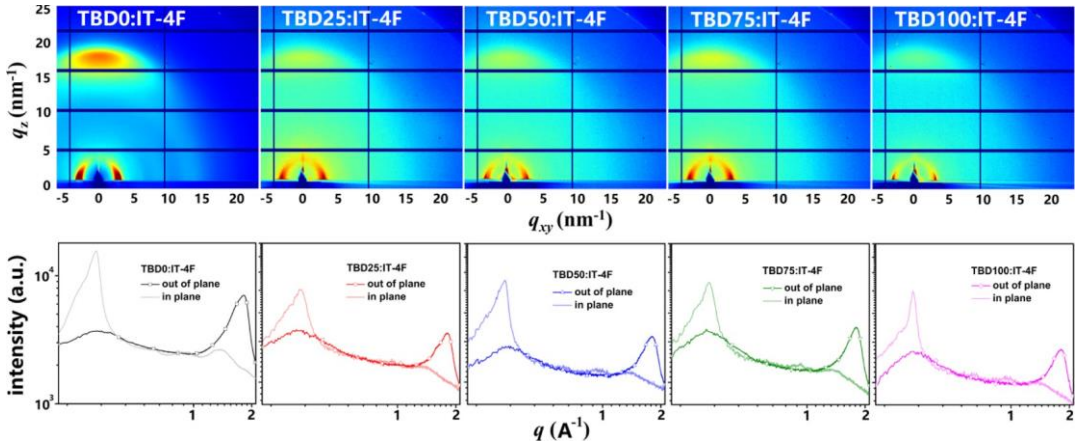

Figure 4. 2D GIWAXS patterns of corresponding polymer:IT-4F films and the related IP and OOP line-cut profiles of the blend films.

with the small difference (±0.02 V) of their V_{oc} (Figure S7). Also, it is clear that there is a small effect on the V_{oc} loss with the variational TBD−TBF composition in terpolymers. Photoluminescence (PL) quenching experiments were carried out to further explore the dissociation and photoinduced CT in TBD*x*:IT-4F blend films. As shown in Figure 3c, when excited at 550 nm, all PL peaks of the polymers in the blend films were efficiently quenched, indicating the efficient electron transfer from the polymer donor to the electron acceptor for excitons generated in the donor phase, and converted to photocurrent, although the energetic offset between E_g and E_{CT} is negligible for the TBD*x*:IT-4F system.

To clarify the relationship between morphology and various compositions of TBD−TBF segments in the polymer backbone, transmission electron microscopy (TEM) and GIWAXS measurement were performed. As shown in Figure S8, TBD0/IT-4F shows a coarse and inhomogeneous phase separation across the entire area, which could be attributed to the polymer or IT-4F rich region. Such excessive aggregation may tend to favor recombination, leading to reduced photocurrent. With the gradual embedding of the TBD segment into the copolymer, the reduced single fraction concentration and formation of a nanoscale interconnected network beneficial for charge transport, such as the TBD50/IT-4F blend, can result in improved J_{sc} and FF values.[63] From GIWAXS results (Figure 4), one can observe that all blend films exhibit resembling profiles in both IP and OOP orientations with a predominant face-on orientation, which is similar to that of neat films, indicating that TBD*x*:IT-4F blend films can largely retain the orientation of neat polymer films (Figure S5c). The high crystallinity of TBD0:IT-4F may be ascribed to the strong aggregation of the donor material and result in excessive phase separation, which is in accordance with the observation in TEM characterizations. In addition, with the increasing TBD content in the polymer TBD0 backbone, the intensity of the (010) stacking gradually declines and the π−π stacking distance successively increased from 3.51 Å (TBD0) to 3.70 Å (TBD100). In a word, the results agree with the well-developed conception that the incorporated TBD segment can inhibit the strong aggregation of blend films and optimize the nanophase separation, along with the retained face-on orientation geometry, which is favorable for photovoltaic application.

Subsequently, GI small-angle X-ray scattering (GISAXS) was employed to further obtain more detailed information on the variation of the nanoscale aggregation and phase separation of the blend films when the TBD−TBF composition changed (Figure S9).[64−66] The curves are fitted to the data using a universal model (described in detail in the Supporting Information). All the parameters obtained from GISAXS analysis are summarized in Table 2, where ξ is the average correlation length of the polymer phase and η and D are the correlation length and fractal dimension of IT-4F aggregates. The Guinier radius (R_g) represents the size of clustered IT-4F aggregates, which is estimated by the equation

$$R_g = \sqrt{\frac{D \times (D+1)}{2}}\,\eta$$

Table 2. Fitting Parameters Obtained from GISAXS 1D Profiles

blend	ξ (nm)	D	η (nm)	$2R_g$ (nm)
TBD0:IT-4F	51.5	2.92	6.9	30.3
TBD25:IT-4F	41.8	2.71	5.7	25.6
TBD50:IT-4F	27.8	2.98	3.7	18.0
TBD75:IT-4F	31.6	2.77	2.9	13.1
TBD100:IT-4F	36.6	2.80	2.1	9.8

As shown in Table 2, the TBD0:IT-4F film exhibits a large correlation length of 51.5 nm, which is reduced along with the certain insertion of TBD (≤50%) but slightly increased when the weight ratio of TBD is over 0.5. Although the large polymer domains are beneficial for charge transport in the active layer, they also cause the formation of a diffuse interface between the polymer and IT-4F domains (such as TBD0) and hinder exciton dissociation, which is consistent with the TEM and GIWAXS results.[35,67] Meanwhile, both η and $2R_g$, which represent IT-4F clusters, are decreased with an increase of TBD content in the terpolymer, and proper values of 3.7 and 18.0 nm are acquired for the TBD50 blend film. Considering the above results, one can speculate that adjustment of TBD and TBF proportion in the TBD-based terpolymer is a simple and useful approach to promote the polymer and acceptor with medium-scale phase separation and suitable domain size, facilitating both exciton dissociation and charge transport.

To further probe how the terpolymer strategy influences charge photogeneration and recombination dynamics, we carried out ultrafast transient absorption (TA) spectroscopy which can observe exciton-to-charge conversion.[68,69] TA

https://dx.doi.org/10.1021/acsami.0c01323
ACS Appl. Mater. Interfaces 2020, 12, 20393−20403

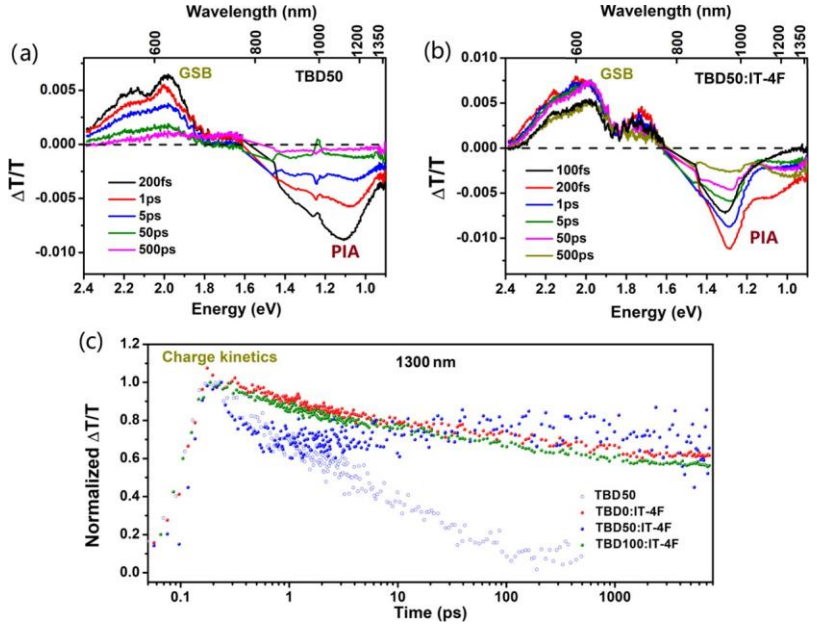

Figure 5. TA spectra of (a) neat TBD50 film and (b) TBD50:IT-4F blend film following excitation at 500 nm (2.48 eV, 2 nJ cm^{-2}). (c) Kinetics for TBDx:IT-4F (0, 50, 100) blend films from the same measurements as part (a) at the wavelength of 1300 nm. TA data for the blend following excitation at 500 nm, where the donor absorbs.

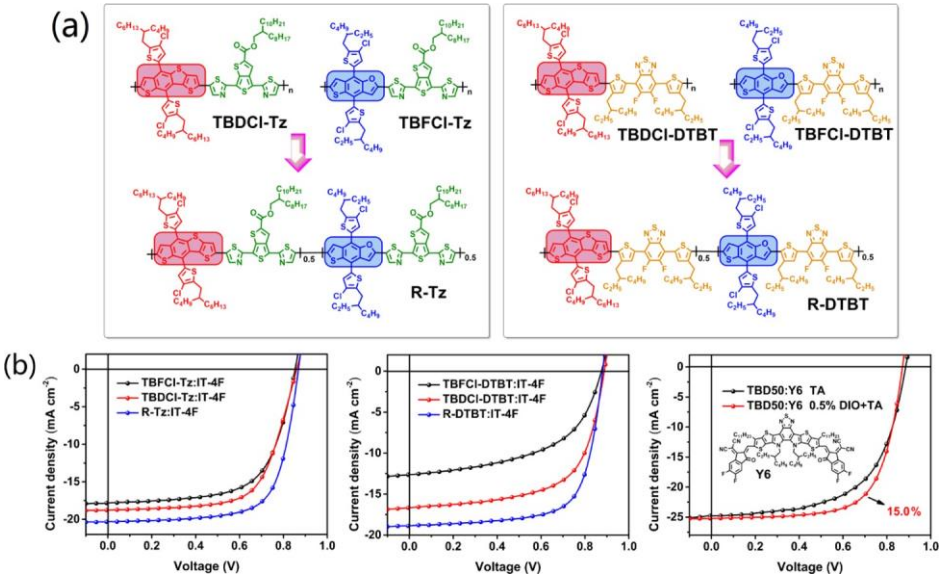

Figure 6. (a) Chemical structures of a new designed TBDx polymer (x = 0, 50, 100) with two electron-deficient units (Tz and DTBT). For terpolymers R-Tz and R-DTBT, the TBD and TBF composition is confirmed to be 1:1. (b) $J-V$ characteristics of PSC devices based on the different polymer/NFA pairs.

spectroscopy can also enable us to establish the link between the blend film morphology and photocurrent generation. For the high-performance polymer TBD50, the TA result in the absence of IT-4F allowed us to first identify exciton signatures and guide the interpretation of spectra and kinetics of blends.[60] In general, the TA spectra consist of three main features: positive signals ($\Delta T/T > 0$) attributed to ground-state bleaching (GSB) signals where the steady-state spectra show prominent absorption bands, negative signals ($\Delta T/T < 0$) derived from photoinduced absorption (PIA, excited state) to high-lying states, and simulated emission signals where the steady-state spectra show fluorescence. For the polymer:IT-4F blend systems, the TA spectra were monitored upon excitation at 500 nm, at which wavelength only the donor materials are selectively excited.

The TA spectra of pure terpolymer TBD50 show a quickly decayed GSB signal in the visible region and a PIA peak at ~1150 nm (1.08 eV, Figure 5a). However, for the TBD50/IT-4F blend film, there is hardly any changed GSB signal at the time scale of 100 ps, indicating efficient electron transfer from TBD to IT-4F on this time scale. In the infrared region, the emergence of a new absorption peak at ~970 nm (1.28 eV) at the earliest delay time (100 fs) can be attributed to the prompt formation of excitons and convert to charge with an additional PIA peak at ~1300 nm (Figure 5b), which persists beyond the nanosecond time scale and is often observed in poly-

https://dx.doi.org/10.1021/acsami.0c01323
ACS Appl. Mater. Interfaces 2020, 12, 20393−20403

Table 3. Device Parameters of the PSCs Based on Different Polymer/NFA Pairs under the Illumination of AM 1.5G, 100 mW cm^{-2}

active layer	V_{oc}[a] (V)	J_{sc}[a] (mA cm^{-2})		FF[a] (%)	PCE[a] (%)
TBFCl−Tz:IT-4F	0.853 (0.849 ± 0.004)	17.8 (17.4 ± 0.4)	17.2	0.644 (0.628 ± 0.017)	9.8 (9.5 ± 0.3)
TBDCl−Tz:IT-4F	0.860 (0.856 ± 0.005)	18.8 (18.5 ± 0.3)	18.0	0.656 (0.637 ± 0.021)	10.6 (10.3 ± 0.3)
R-Tz:IT-4F	0.868 (0.864 ± 0.004)	20.90 (20.4 ± 0.5)	20.0	0.718 (0.705 ± 0.015)	13.0 (12.8 ± 0.2)
TBFCl−DTBT:IT-4F	0.874 (0.872 ± 0.003)	12.62 (12.3 ± 0.3)	12.1	0.533 (0.514 ± 0.016)	6.2 (5.8 ± 0.4)
TBDCl−DTBT:IT-4F	0.887 (0.884 ± 0.004)	16.7 (16.3 ± 0.3)	16.1	0.630 (0.613 ± 0.020)	9.3 (9.0 ± 0.3)
R-DTBT:IT-4F	0.880 (0.877 ± 0.004)	18.8 (18.5 ± 0.3)	18.2	0.712 (0.698 ± 0.014)	11.8 (11.5 ± 0.3)
TBD50:Y6	0.878 (0.876 ± 0.003)	25.1 (24.7 ± 0.5)	24.3	0.680 (0.668 ± 0.015)	15.0 (14.7 ± 0.3)

[a]The values in parentheses are the average values with standard deviations obtained from 15 devices. The thickness of the active layer is 110 ± 15 nm.

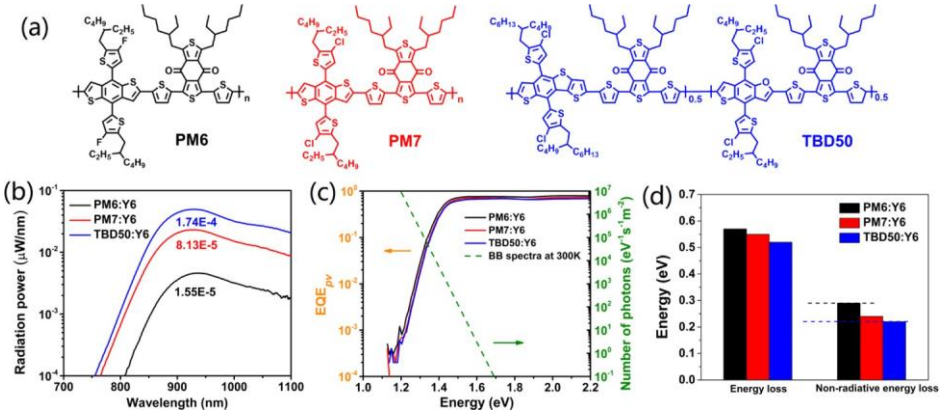

Figure 7. (a) Molecular structure of the state-of-the-art polymer donors PM6 and PM7 and the new polymer TBD50. (b) EL intensity and EQE_{EL} of PM6:Y6, PM7:Y6, and TBD50:Y6 blends at the constant injecting current. (c) Highly sensitive EQE_{PV} spectra and the 300 K blackbody spectra. (d) Energy loss and nonradiative energy loss of the corresponding PSCs.

mer:PCBM systems.[69,70] In addition, the D−A copolymer TBD0 and TBD100 blends show essentially identical spectra (Figures S10 and S11, Supporting Information).

The charge generation and recombination kinetics can be monitored via PIA at ∼1300 nm for the three different blend films in a normalized scale. As shown in Figure 5c, the TBD50/IT-4F blend exhibits prompt charge generation within a 100 fs excitation pulse but shows the earliest decay at the scale of 1 ps. Then, the charge generation process remains constant beyond 5 ns. On the contrary, for TBD0/IT-4F and TBD100/IT-4F blends within the 5 ns window, the total charge population decays gradually in the whole time scale from 100 fs to 5 ns, reflecting the occurrence of higher bimolecular recombination. The results suggest that the existence of the long-lived dissociated excitons in the TBD-A−TBF-A terpolymer blend can reduce the bimolecular recombination, which is beneficial to achieve more efficient photo-to-electron conversions and result in improved device performance.

To illustrate the wide utility of our design terpolymer strategy, we further design new TBD-A−TBF-A terpolymers by using two classical electron-deficient units Tz and DTBT, which comprise an equal molar amount of TBD and TBF, and the corresponding D−A copolymers were synthesized for comparison (Figure 6a). The synthetic details are shown in Scheme S1, and the UV−vis absorption is displayed in Figure S12 in the Supporting Information. It is known that Tz and DTBT are the most successful electron-deficient units in fullerene PSCs. Because of the strong crystallinity of these polymers, their morphology is difficult to regulate when blended with A−D−A-type small-molecule acceptors and not widely used in highly efficient NF-PSCs.[71−73] From the above analysis, our terpolymer strategy can reduce strong aggregation of polymers and modulate molecular packing and phase separation with acceptors. Thus, this strategy may work effectively in DTBT and Tz systems.

The photovoltaic properties of all the different D/A pairs were investigated by fabricating PSCs with a conventional device structure. The optimized treatment condition for active layers is using TA at 110 °C for 10 min with 0.5% DIO as the additive (the optimized D−A ratio is 1:1). The optimal photovoltaic parameters for all the PSCs are summarized in Tables S4 and S5. As expected, by combining the TBF and TBD units in the terpolymer main chain, enhanced PCEs were recorded, in comparison with their respective D−A copolymer devices (Figure 6b and Table 3). As summarized in Tables S4 and S5, the improved device J_{sc} and FF values are observed in all the terpolymer devices. Notably, the R-Tz:IT-4F and R-DTBT:IT-4F devices yield promising efficiencies of 13.0 and 11.8%, which are both high values reported for Tz- and DTBT-based polymers. Then, we examined the morphology of Tz-based three blends through the GIWAXS measurement, as shown in Figure S13. As our assumption, the three polymers showed a consistent trend where the crystallinity weakened by replacing 50% TBF with the TBD segment.

Subsequently, we extend our study beyond acceptor IT-4F and select a recently reported small molecular acceptor Y6, which shows ultrahigh efficiency when combining with a few BDT-based donor materials in the literature (the molecular structure of Y6 is shown in Figure 6b).[10,30,33,74] With our terpolymer approach, the organic photovoltaic device based on the new material pair TBD50:Y6 affords a PCE of 15.0%

https://dx.doi.org/10.1021/acsami.0c01323
ACS Appl. Mater. Interfaces 2020, 12, 20393−20403

Table 4. Measured and Calculated Parameters To Quantify the Nonradiative Recombination Losses of the PM6:Y6, PM7:Y6, and TBD50:Y6-Based PSCs

device	E_g[a] (eV)	$V_{oc,SQ}$ (V)	$V_{oc,rad}$[b] (V)	$V_{oc,meas}$ (V)	$E_g/q - V_{oc}$ (V)	$\Delta V_{oc,nr}$[c] (V)	$\Delta V_{oc,nr}$[d] (V)
PM6:Y6	1.40	1.14	1.09	0.83	0.57	0.26	0.287
PM7:Y6	1.40	1.14	1.08	0.85	0.55	0.23	0.244
TBD50:Y6	1.40	1.14	1.09	0.88	0.52	0.21	0.225

[a]E_g was determined from the intersection of the EQE edge and the local EQE maximum.[60] [b]$V_{oc,rad} = kT/q \ln(J_{sc}/J_{0,rad} + 1)$. [c]$\Delta V_{oc,nr} = V_{oc,rad} - V_{oc,meas}$. [d]$\Delta V_{oc,nr} = -(kt/q)\ln(EQE_{EL})$.

(Table 3), which is very close to the typical device performance in the PM6:Y6 system (15.7%).[10] Notably, an impressive V_{oc} of 0.88 V is obtained in the TBD50:Y6-based device, higher than that of PM6:Y6 (0.84 V) and PM7:Y6 (0.86 V) (Figure 7a). The estimated E_{loss}, defined as $E_{loss} = E_g - qV_{oc}$, is only 0.52 eV in the TBD50:Y6-based device, which is significantly smaller than most reported E_{loss} (the band gap of Y6 is determined to be 1.40 eV from the intersection of the extrapolated EQE edge and the local EQE maximum at the edge of the EQE spectrum, Figure S14).[75]

Finally, to figure out the intrinsic reason why the TBD50:Y6-based devices achieved lower E_{loss} relative to those of the PM6:Y6- and PM7:Y6-based devices, we perform detailed device physics analyses. According to the Shockley–Queisser (SQ) theory,[76] as shown in eq 1, the SQ limit, $V_{oc,SQ}$, for all the three different blend systems are 1.14 V.

$$V_{oc}^{SQ} = \frac{kt}{q}\ln\left(\frac{J_{sc}}{J_0^{SQ}} + 1\right) J_0^{SQ} = q\cdot\int_{E_{gap}}^{\infty} \varnothing_{BB}(E)\,dE \quad (1)$$

The radiative V_{oc} limit, $V_{oc,rad}$, originating from radiative recombination loss below the band gap can be calculated by combining EQE_{PV} and EL spectroscopy (Figure 7b,c) using eq 2[77]

$$V_{oc}^{rad} = \frac{kt}{q}\ln\left(\frac{J_{sc}}{J_0^{rad}} + 1\right) J^{rad} = q\cdot\int_0^{\infty} EQE_{PV}\,\varnothing_{BB}(E)\,dE \quad (2)$$

As shown in Table 4, the $V_{oc,rad}$ is calculated to be 1.09, 1.08, and 1.09 V for the PM6/Y6, PM7/Y6, and TBD50/Y6-based devices.

The nonradiative V_{oc} loss ($\Delta V_{oc,nr}$), which is the difference between $V_{oc,rad}$ and the measured V_{oc} ($V_{oc,meas}$) under 1 sun illumination, is 0.21 V for the TBD50:Y6-based device, lower than those for PM6:Y6 (0.26 V) and PM7:Y6 (0.23 V) devices. To further verify the detailed parameter of $\Delta V_{oc,nr}$, the EL quantum efficiency (EQE_{EL}) of the relevant solar cells was measured, which can be calculated via another eq 3[23]

$$\Delta V_{oc,nr} = -\frac{kt}{q}\ln(EQE_{EL}) \quad (3)$$

The $\Delta V_{oc,nr}$ is inversely related to EQE_{EL}. As shown in Figure 7b, the device based on TBD50:Y6 exhibits the highest EQE_{EL} value of 1.74×10^{-4} than the PM6:Y6 and PM7:Y6 devices, which is among the highest value in NF-PSCs, implying the extremely low nonradiative recombination loss of 0.225 eV in the TBD50:Y6 device (see Table 4). Figure 7d displays the energy loss and nonradiative energy loss of the three different blends. By the detailed comparison of the state-of-the-art PM6:Y6 and PM7:Y6 devices, the higher V_{oc} and low

exploitation and utilization of the advantages of TBD and TBF moieties, this new terpolymer methodology has been found to hold great potential to suppress nonradiative recombination loss, thus improving V_{oc} in PSCs.

By combining the above morphology analyses, charge dynamics and energy loss measurements, we elaborated the advantages for this new terpolymer methodology: (i) for pure polymer, the smaller atomic radius of oxygen with intense electronegativity in the asymmetric TBF unit can guarantee a more planar polymer backbone. When the TBF unit was inserted into the TBD-based polymer main chain, the strong O···S noncovalent attractive interactions are promoted and the π−π stacking distance is reduced, endowing a terpolymer with higher order orientation and crystallinity; (ii) in blend films, the random incorporated dual-oriented asymmetric TBD unit can break excessive aggregated polymer domains and allow small molecular acceptors to penetrate into the large polymer domains. The reasonable TBD−TBF ratio in the terpolymer main chain can result in a balanced miscibility and phase separation between the donor and acceptor, which facilitates charge transport, reduces charge recombination, and leads to high photovoltaic performance. (iii) Integrating two asymmetric TBF and TBD segments is a potential terpolymer methodology for designing NF-PSCs with low nonradiative energy loss.

CONCLUSIONS

In conclusion, we put forward a facile terpolymer strategy to design a series of new polymers and systematically investigate the relationship between molecular structure, morphology, energy loss, and photovoltaic performance. The key of this strategy involves the use of two asymmetric segments, TBF and TBD, inducing synergetic effect on the blend films: the TBF segment is utilized to keep the dense molecular stacking, while the TBD moiety is expected to inhibit the formation of strong aggregation of the blend films and modulate nonradiative energy loss. By precise tailoring the ratio of TBD and TBF segments, enhanced PCEs over 14% were achieved in the TBD50/IT-4F device and outperformed the corresponding D−A copolymers. The controlled domain size, optimized phase separation, and better interpenetrating network of the TBD50/IT-4F blend film can enable efficient exciton energy loss in the TBD50:Y6 device are mainly caused by low nonradiative energy loss. Thus, it can be concluded that by full

https://dx.doi.org/10.1021/acsami.0c01323
ACS Appl. Mater. Interfaces 2020, 12, 20393−20403

dissociation and suppress carrier recombination, along with high yields of long-lived charges. Moreover, investigations of different polymer/NFA pairs manifested that our strategy can be applicable to substantial conjugated polymers and accept- ors, especially in a strong aggregation system. Significantly, an impressive V_{oc} of 0.88 V is achieved in the TBD50/Y6 device at a band gap of 1.40 eV, and the E_{loss} is only 0.52 eV. Compared with PM6/Y6 and PM7/Y6, the higher EQE_{EL} value of 1.74×10^{-4} for TBD50/Y6 blends demonstrates a low nonradiative recombination loss of 0.22 eV, leading to the increase in V_{oc}. Thus, our results demonstrate a new

https://dx.doi.org/10.1021/acsami.0c01323
ACS Appl. Mater. Interfaces 2020, 12, 20393−20403

terpolymer methodology with backbone engineering to provide more possibilities to improve PCE and enrich diversity and broaden the available candidates for new p-type polymers in the field of organic solar cells.

EXPERIMENTAL SECTION

Materials. All the reagents, unless otherwise specified, were purchased from Sigma-Aldrich Co., J&K, and Tokyo Chemical Industry Co., Ltd. and were used without further purification. The synthesis details of the monomers and polymers are collected in the Supporting Information.

ASSOCIATED CONTENT

Supporting Information

The Supporting Information is available free of charge at https://pubs.acs.org/doi/10.1021/acsami.0c01323.

Experimental details for the synthesis of materials, material characterization, device fabrication and characterization, and mobility measurement (PDF)

AUTHOR INFORMATION

Corresponding Authors

Chunming Yang − *Shanghai Synchrotron Radiation Facility, Shanghai Institute of Applied Physics, Chinese Academy of Sciences, Shanghai 201204, China;* orcid.org/0000-0001-8008-3675; Email: yangchunming@zjlab.org.cn

Xichang Bao − *CAS Key Laboratory of Bio-based Materials, Qingdao Institute of Bioenergy and Bioprocess Technology, Chinese Academy of Sciences, Qingdao 266101, China;* orcid.org/0000-0001-7325-7550; Email: baoxc@qibebt.ac.cn

Renqiang Yang − *CAS Key Laboratory of Bio-based Materials, Qingdao Institute of Bioenergy and Bioprocess Technology, Chinese Academy of Sciences, Qingdao 266101, China;* orcid.org/0000-0001-6794-7416; Email: yangrq@qibebt.ac.cn

Authors

Xunchang Wang − *CAS Key Laboratory of Bio-based Materials, Qingdao Institute of Bioenergy and Bioprocess Technology, Chinese Academy of Sciences, Qingdao 266101, China; Center of Materials Science and Optoelectronics Engineering, University of Chinese Academy of Sciences, Beijing 100049, China*

Jianhua Han − *CAS Key Laboratory of Bio-based Materials, Qingdao Institute of Bioenergy and Bioprocess Technology, Chinese Academy of Sciences, Qingdao 266101, China*

Da Huang − *Shanghai Synchrotron Radiation Facility, Shanghai Institute of Applied Physics, Chinese Academy of Sciences, Shanghai 201204, China*

Jianing Wang − *Guangdong Provincial Key Laboratory of Nanophotonic Functional Materials and Devices, Institute of Semiconductor Science and Technology, South China Normal University, Guangzhou 510631, China*

Yuan Xie − *Institute of Polymer Optoelectronic Materials and Devices, State Key Laboratory of Luminescent Materials and Devices, South China University of Technology, Guangzhou 510640, China*

Zhilin Liu − *CAS Key Laboratory of Bio-based Materials, Qingdao Institute of Bioenergy and Bioprocess Technology, Chinese Academy of Sciences, Qingdao 266101, China*

Yonghai Li − *CAS Key Laboratory of Bio-based Materials, Qingdao Institute of Bioenergy and Bioprocess Technology, Chinese Academy of Sciences, Qingdao 266101, China;* orcid.org/0000-0002-5748-0258

Yong Zhang − *Guangdong Provincial Key Laboratory of Nanophotonic Functional Materials and Devices, Institute of Semiconductor Science and Technology, South China Normal University, Guangzhou 510631, China;* orcid.org/0000-0001-7718-5945

Zhicai He − *Institute of Polymer Optoelectronic Materials and Devices, State Key Laboratory of Luminescent Materials and Devices, South China University of Technology, Guangzhou 510640, China*

Complete contact information is available at: https://pubs.acs.org/10.1021/acsami.0c01323

Notes

The authors declare no competing financial interest.

ACKNOWLEDGMENTS

The authors are deeply grateful to the National Natural Science Foundation of China (51773220, 51573205, and 21502205), Youth Innovation Promotion Association CAS (2016194), DICP & QIBEBT (UN201709 and UN201805), and Dalian National Laboratory for Clean Energy (DNL) CAS for financial support.

REFERENCES

(1) Yu, G.; Gao, J.; Hummelen, J. C.; Wudl, F.; Heeger, A. J. Polymer Photovoltaic Cells: Enhanced Efficiencies via a Network of Internal Donor-Acceptor Heterojunctions. *Science* 1995, *270*, 1789−1791.

(2) Espinosa, N.; Hösel, M.; Jørgensen, M.; Krebs, F. C. Large Scale Deployment of Polymer Solar Cells on Land, on Sea and in the Air. *Energy Environ. Sci.* 2014, *7*, 855−866.

(3) Dou, L.; Liu, Y.; Hong, Z.; Li, G.; Yang, Y. Low-Bandgap Near-IR Conjugated Polymers/Molecules for Organic Electronics. *Chem. Rev.* 2015, *115*, 12633−12665.

(4) He, Z.; Xiao, B.; Liu, F.; Wu, H.; Yang, Y.; Xiao, S.; Wang, C.; Russell, T. P.; Cao, Y. Single-Junction Polymer Solar Cells with High Efficiency and Photovoltage. *Nat. Photonics* 2015, *9*, 174−179.

(5) Dennler, G.; Scharber, M. C.; Brabec, C. J. Polymer-Fullerene Bulk-Heterojunction Solar Cells. *Adv. Mater.* 2009, *21*, 1323−1338.

(6) Li, Y. Molecular Design of Photovoltaic Materials for Polymer Solar Cells: Toward Suitable Electronic Energy Levels and Broad Absorption. *Acc. Chem. Res.* 2012, *45*, 723−733.

(7) Li, G.; Zhu, R.; Yang, Y. Polymer Solar Cells. *Nat. Photonics* 2012, *6*, 153−161.

(8) Yan, C.; Barlow, S.; Wang, Z.; Yan, H.; Jen, A. K. Y.; Marder, S. R.; Zhan, X. Non-Fullerene Acceptors for Organic Solar Cells. *Nat. Rev. Mater.* 2018, *3*, 18003.

(9) Lin, Y.; Wang, J.; Zhang, Z.-G.; Bai, H.; Li, Y.; Zhu, D.; Zhan, X. An Electron Acceptor Challenging Fullerenes for Efficient Polymer Solar Cells. *Adv. Mater.* 2015, *27*, 1170−1174.

(10) Yuan, J.; Zhang, Y.; Zhou, L.; Zhang, G.; Yip, H.-L.; Lau, T.-K.; Lu, X.; Zhu, C.; Peng, H.; Johnson, P. A.; Leclerc, M.; Cao, Y.; Ulanski, J.; Li, Y.; Zou, Y. Single-Junction Organic Solar Cell with over 15% Efficiency Using Fused-Ring Acceptor with Electron-Deficient Core. *Joule* 2019, *3*, 1140−1151.

(11) Cui, C.; Li, Y. High-Performance Conjugated Polymer Donor Materials for Polymer Solar Cells with Narrow Bandgap Nonfullerene Acceptors. *Energy Environ. Sci.* 2019, *12*, 3225−3246.

(12) Hou, J.; Inganäs, O.; Friend, R. H.; Gao, F. Organic Solar Cells Based on Non-Fullerene Acceptors. *Nat. Mater.* 2018, *17*, 119−128.

(13) Xu, X.; Feng, K.; Bi, Z.; Ma, W.; Zhang, G.; Peng, Q. Single-Junction Polymer Solar Cells with 16.35% Efficiency Enabled by a Platinum(II) Complexation Strategy. *Adv. Mater.* 2019, *31*, 1901872.

(14) Li, Y.; Zheng, N.; Yu, L.; Wen, S.; Gao, C.; Sun, M.; Yang, R. A Simple Phenyl Group Introduced at the Tail of Alkyl Side Chains of Small Molecular Acceptors: New Strategy to Balance the Crystallinity of Acceptors and Miscibility of Bulk Heterojunction Enabling Highly Efficient Organic Solar Cells. *Adv. Mater.* 2019, *31*, 1807832.
(15) Li, K.; Wu, Y.; Tang, Y.; Pan, M. A.; Ma, W.; Fu, H.; Zhan, C.; Yao, J. Ternary Blended Fullerene-Free Polymer Solar Cells with 16.5% Efficiency Enabled with a Higher-LUMO-Level Acceptor to Improve Film Morphology. *Adv. Energy Mater.* 2019, *9*, 1901728.
(16) Yan, T.; Song, W.; Huang, J.; Peng, R.; Huang, L.; Ge, Z. 16.67% Rigid and 14.06% Flexible Organic Solar Cells Enabled by Ternary Heterojunction Strategy. *Adv. Mater.* 2019, *31*, 1902210.
(17) Cui, Y.; Yao, H.; Zhang, J.; Zhang, T.; Wang, Y.; Hong, L.; Xian, K.; Xu, B.; Zhang, S.; Peng, J.; Wei, Z.; Gao, F.; Hou, J. Over 16% Efficiency Organic Photovoltaic Cells Enabled by a Chlorinated Acceptor with Increased Open-Circuit Voltages. *Nat. Commun.* 2019, *10*, 2515.
(18) Liu, Q.; Jiang, Y.; Jin, K.; Qin, N.; Xu, J.; Li, W.; Xiong, J.; Liu, J.; Sun, K.; Yang, S.; Zhang, X.; Ding, L. 18% Efficiency Organic Solar Cells. *Sci. Bull.* 2020, *65*, 272−275.
(19) Liu, L.; Kan, Y.; Gao, K.; Wang, J.; Zhao, M.; Chen, H.; Zhao, C.; Jiu, T.; Jen, A.; Li, Y. Graphdiyne Derivative as Multifunctional Solid Additive in Binary Organic Solar Cells with 17.3% Efficiency and High Reproductivity. *Adv. Mater.* 2020, *32*, 1907604.
(20) Zhan, L.; Li, S.; Lau, T.; Cui, Y.; Lu, X.; Shi, M.; Li, C.; Li, H.; Hou, J.; Chen, H. Over 17% Efficiency Ternary Organic Solar Cells Enabled by Two Non-Fullerene Acceptors Working in an Alloy-Like Model. *Energy Environ. Sci.* 2020, *13*, 635−645.
(21) Meng, L.; Zhang, Y.; Wan, X.; Li, C.; Zhang, X.; Wang, Y.; Ke, X.; Xiao, Z.; Ding, L.; Xia, R.; Yip, H.; Cao, Y.; Chen, Y. Organic and Solution-Processed Tandem Solar Cells with 17.3% Efficiency. *Science* 2018, *361*, 1094−1098.
(22) Ye, L.; Zhang, S.; Huo, L.; Zhang, M.; Hou, J. Molecular Design Toward Highly Efficient Photovoltaic Polymers Based on Two-Dimensional Conjugated Benzodithiophene. *Acc. Chem. Res.* 2014, *47*, 1595−1603.
(23) Zhao, W.; Qian, D.; Zhang, S.; Li, S.; Inganas̈, O.; Gao, F.; Hou, J. Fullerene-Free Polymer Solar Cells with over 11% Efficiency and Excellent Thermal Stability. *Adv. Mater.* 2016, *28*, 4734−4739.
(24) Zhang, M.; Guo, X.; Ma, W.; Ade, H.; Hou, J. A Large-Bandgap Conjugated Polymer for Versatile Photovoltaic Applications with High Performance. *Adv. Mater.* 2015, *27*, 4655−4660.
(25) Zhao, J.; Li, Y.; Yang, G.; Jiang, K.; Lin, H.; Ade, H.; Ma, W.; Yan, H. Efficient Organic Solar Cells Processed from Hydrocarbon Solvents. *Nat. Energy* 2016, *1*, 15027.
(26) Jiang, H.; Li, X.; Wang, H.; Ren, Z.; Zheng, N.; Wang, X.; Li, Y.; Chen, W.; Yang, R. Significantly Enhanced Molecular Stacking in Ternary Bulk Heterojunctions Enabled by an Appropriate Side Group on Donor Polymer. *Adv. Sci.* 2020, *7*, 1903455.
(27) Li, S.; Ye, L.; Zhao, W.; Yan, H.; Yang, B.; Liu, D.; Li, W.; Ade, H.; Hou, J. A Wide Band Gap Polymer with a Deep Highest Occupied Molecular Orbital Level Enables 14.2% Efficiency in Polymer Solar Cells. *J. Am. Chem. Soc.* 2018, *140*, 7159−7167.
(28) Li, J.; Wang, Y.; Liang, Z.; Qin, J.; Ren, M.; Tong, J.; Yang, C.; Yang, C.; Bao, X.; Xia, Y. Non-toxic green food additive enables efficient polymer solar cells through adjusting the phase composition distribution and boosting charge transport. *J. Mater. Chem. C* 2020, *8*, 2483−2490.
(29) Sun, C.; Pan, F.; Bin, H.; Zhang, J.; Xue, L.; Qiu, B.; Wei, Z.; Zhang, Z.; Li, Y. A Low Cost and High Performance Polymer Donor Material for Polymer Solar Cells. *Nat. Commun.* 2018, *9*, 743.
(30) Sun, C.; Pan, F.; Chen, S.; Wang, R.; Sun, R.; Shang, Z.; Qiu, B.; Min, J.; Lv, M.; Meng, L.; Zhang, C.; Xiao, M.; Yang, C.; Li, Y. Achieving Fast Charge Separation and Low Nonradiative Recombination Loss by Rational Fluorination for High-Efficiency Polymer Solar Cells. *Adv. Mater.* 2019, *31*, 1905480.
(31) Xu, X.; Feng, K.; Lee, Y. W.; Woo, H. Y.; Zhang, G.; Peng, Q. Subtle Polymer Donor and Molecular Acceptor Design Enable Efficient Polymer Solar Cells with a Very Small Energy Loss. *Adv. Funct. Mater.* 2020, *30*, 1907570.
(32) Yu, J.; Chen, P.; Woo, C.; Koh, W.; Wang, H.; Yang, K.; Zhou, X.; Liu, B.; Liao, Q.; Chen, J.; Sun, H.; Woo, H.; Zhang, S.; Guo, X. Phthalimide-Based High Mobility Polymer Semiconductors for Efficient Nonfullerene Solar Cells with Power Conversion Efficiencies over 13%. *Adv. Sci.* 2019, *6*, 1801743.
(33) Sun, H.; Liu, T.; Yu, J.; Lau, T.; Zhang, G.; Zhang, G.; Zhang, Y.; Sun, M.; Tang, Y.; Ma, R.; Liu, B.; Liang, J.; Feng, K.; Lu, X.; Guo, X.; Gao, F.; Yan, H. A Monothiophene Unit Incorporating both Fluoro and Ester Substitution Enabling High-Performance Donor Polymers for Non-Fullerene Solar Cells with 16.4% Efficiency. *Energy Environ. Sci.* 2019, *12*, 3328−3337.
(34) Bin, H.; Gao, L.; Zhang, Z. G.; Yang, Y.; Zhang, Y.; Zhang, C.; Chen, S.; Xue, L.; Yang, C.; Xiao, M.; Li, Y. 11.4% Efficiency Non-Fullerene Polymer Solar Cells with Trialkylsilyl Substituted 2D-Conjugated Polymer as Donor. *Nat. Commun.* 2016, *7*, 13651.
(35) Liu, D.; Wang, J.; Gu, C.; Li, Y.; Bao, X.; Yang, R. Stirring Up Acceptor Phase and Controlling Morphology via Choosing Appropriate Rigid Aryl Rings as Lever Arms in Symmetry-Breaking Benzodithiophene for High-Performance Fullerene and Fullerene-Free Polymer Solar Cells. *Adv. Mater.* 2018, *30*, 1705870.
(36) Liu, T.; Pan, X.; Meng, X.; Liu, Y.; Wei, D.; Ma, W.; Huo, L.; Sun, X.; Lee, T. H.; Huang, M.; Choi, H.; Kim, J. Y.; Choy, W. C.; Sun, Y. Alkyl Side-Chain Engineering in Wide-Bandgap Copolymers Leading to Power Conversion Efficiencies over 10%. *Adv. Mater.* 2017, *29*, 1604251.
(37) Liao, Z.; Xie, Y.; Chen, L.; Tan, Y.; Huang, S.; An, Y.; Ryu, H. S.; Meng, X.; Liao, X.; Huang, B.; Xie, Q.; Woo, H. Y.; Sun, Y.; Chen, Y. Fluorobenzotriazole (FTAZ)-Based Polymer Donor Enables Organic Solar Cells Exceeding 12% Efficiency. *Adv. Funct. Mater.* 2019, *29*, 1808828.
(38) Fu, H.; Wang, Z.; Sun, Y. Polymer Donors for High-Performance Non-Fullerene Organic Solar Cells. *Angew. Chem., Int. Ed.* 2019, *58*, 4442−4453.
(39) An, L.; Tong, J.; Huang, Y.; Liang, Z.; Li, J.; Yang, C.; Wang, X. Elevated Photovoltaic Performance in Medium Bandgap Copolymers Composed of Indacenodi-thieno[3,2-b]thiophene and Benzothiadiazole Subunits by Modulating the π-Bridge. *Polymers* 2020, *12*, 368.
(40) Ye, L.; Zhang, S.; Zhao, W.; Yao, H.; Hou, J. Highly Efficient 2D-Conjugated Benzodithiophene-Based Photovoltaic Polymer with Linear Alkylthio Side Chain. *Chem. Mater.* 2014, *26*, 3603−3605.
(41) Zhu, D.; Bao, X.; Zhu, Q.; Gu, C.; Qiu, M.; Wen, S.; Wang, J.; Shahid, B.; Yang, R. Thienothiophene-based copolymers for high-performance solar cells, employing different orientations of the thiazole group as a π bridge. *Energy Environ. Sci.* 2017, *10*, 614−620.
(42) Chen, W.; Huang, G.; Li, X.; Li, Y.; Wang, H.; Jiang, H.; Zhao, Z.; Yu, D.; Wang, E.; Yang, R. Revealing the Position Effect of an Alkylthio Side Chain in Phenyl-Substituted Benzodithiophene-Based Donor Polymers on the Photovoltaic Performance of Non-Fullerene Organic Solar Cells. *ACS Appl. Mater. Interfaces* 2019, *11*, 33173−33178.
(43) Li, X.; Huang, G.; Chen, W.; Jiang, H.; Qiao, S.; Yang, R. Size Effect of Two Dimension Conjugated Space in Photovoltaic Polymers' Side-chain: Balancing Phase Separation and Charge Transport. *ACS Appl. Mater. Interfaces* 2020, *12*, 16670.
(44) Dang, D.; Yu, D.; Wang, E. Conjugated Donor-Acceptor Terpolymers Toward High-Efficiency Polymer Solar Cells. *Adv. Mater.* 2019, *31*, 1807019.
(45) Hwang, Y.-J.; Earmme, T.; Courtright, B. A. E.; Eberle, F. N.; Jenekhe, S. A. n-Type Semiconducting Naphthalene Diimide-Perylene Diimide Copolymers: Controlling Crystallinity, Blend Morphology, and Compatibility Toward High-Performance All-Polymer Solar Cells. *J. Am. Chem. Soc.* 2015, *137*, 4424−4434.
(46) Ye, L.; Jiao, X.; Zhang, S.; Yao, H.; Qin, Y.; Ade, H.; Hou, J. Control of Mesoscale Morphology and Photovoltaic Performance in Diketopyrrolopyrrole-Based Small Band Gap Terpolymers. *Adv. Energy Mater.* 2017, *7*, 1601138.

https://dx.doi.org/10.1021/acsami.0c01323
ACS Appl. Mater. Interfaces 2020, 12, 20393−20403

(47) Xie, Q.; Liao, X.; Chen, L.; Zhang, M.; Gao, K.; Huang, B.; Xu, H.; Liu, F.; Jen, A. K. Y.; Chen, Y. Random Copolymerization Realized High Efficient Polymer Solar Cells with a Record Fill Factor near 80%. *Nano Energy* 2019, *61*, 228−235.
(48) Chen, S.; Cho, H. J.; Lee, J.; Yang, Y.; Zhang, Z.-G.; Li, Y.; Yang, C. Modulating the Molecular Packing and Nanophase Blending via a Random Terpolymerization Strategy toward 11% Efficiency Nonfullerene Polymer Solar Cells. *Adv. Energy Mater.* 2017, *7*, 1701125.
(49) Wang, X.; Dou, K.; Shahid, B.; Liu, Z.; Li, Y.; Sun, M.; Zheng, N.; Bao, X.; Yang, R. Terpolymer Strategy toward High-Efficiency Polymer Solar Cells: Integrating Symmetric Benzodithiophene and Asymmetrical Thieno[2,3-f]benzofuran Segments. *Chem. Mater.* 2019, *31*, 6163−6173.
(50) Li, J.; Liang, Z.; Li, X.; Li, H.; Wang, Y.; Qin, J.; Tong, J.; Yan, L.; Bao, X.; Xia, Y. Insights into Excitonic Dynamics of Terpolymer-Based High-Efficiency Nonfullerene Polymer Solar Cells: Enhancing the Yield of Charge Separation States. *ACS Appl. Mater. Interfaces* 2020, *12*, 8475−8484.
(51) Cui, Y.; Yao, H.; Hong, L.; Zhang, T.; Xu, Y.; Xian, K.; Gao, B.; Qin, Y.; Zhang, J.; Wei, Z.; Hou, J. Achieving over 15% Efficiency in Organic Photovoltaic Cells via Copolymer Design. *Adv. Mater.* 2019, *31*, 1808356.
(52) Han, J.; Shi, W.; Wang, X.; Cai, J.; Hao, X.; Shi, J.; Bao, X.; Yang, R. Functional Transformation of Four-Bladed Rylene Propellers Utilizing Non-Metal and d^8 Metal Core Shifting Strategy: Significant Impact on Photovoltaic Performance and Electrocatalytic Hydrogen Evolution Activity. *J. Mater. Chem. A* 2020, *8*, 3918−3932.
(53) Wang, X.; Du, Z.; Dou, K.; Jiang, H.; Gao, C.; Han, L.; Yang, R. A Maverick Asymmetrical Backbone with Distinct Flanked Twist Angles Modulating the Molecular Aggregation and Crystallinity for High Performance Nonfullerene Solar Cells. *Adv. Energy Mater.* 2019, *9*, 1802530.
(54) Qiu, L.; Peng, H.; Liu, Y.; Qiu, B.; Zhang, Z.-G.; Li, Y.; Zou, Y. Asymmetric Medium Bandgap Copolymers and Narrow Bandgap Small-Molecule Acceptor with over 7% Efficiency. *Org. Electron.* 2017, *45*, 42−48.
(55) Wang, X.; Dou, K.; Shahid, B.; Liu, Z.; Li, Y.; Sun, M.; Zheng, N.; Bao, X.; Yang, R. Terpolymer Strategy toward High-Efficiency Polymer Solar Cells: Integrating Symmetric Benzodithiophene and Asymmetrical Thieno[2,3-f]benzofuran Segments. *Chem. Mater.* 2019, *31*, 6163−6173.
(56) Huang, P.; Du, J.; Biewer, M. C.; Stefan, M. C. Developments of Furan and Benzodifuran Semiconductors for Organic Photovoltaics. *J. Mater. Chem. A* 2015, *3*, 6244−6257.
(57) Zhao, W.; Li, S.; Yao, H.; Zhang, S.; Zhang, Y.; Yang, B.; Hou, J. Molecular Optimization Enables over 13% Efficiency in Organic Solar Cells. *J. Am. Chem. Soc.* 2017, *139*, 7148−7151.
(58) Wu, J.-L.; Chen, F.-C.; Hsiao, Y.-S.; Chien, F.-C.; Chen, P.; Kuo, C.-H.; Huang, M. H.; Hsu, C.-S. Surface Plasmonic Effects of Metallic Nanoparticles on the Performance of Polymer Bulk Heterojunction Solar Cells. *ACS Nano* 2011, *5*, 959−967.
(59) Cowan, S. R.; Roy, A.; Heeger, A. J. Recombination in Polymer-Fullerene Bulk Heterojunction Solar Cells. *Phys. Rev. B: Condens. Matter Mater. Phys.* 2010, *82*, 245207.
(60) Menke, S. M.; Ran, N. A.; Bazan, G. C.; Friend, R. H. Understanding Energy Loss in Organic Solar Cells: Toward a New Efficiency Regime. *Joule* 2018, *2*, 25−35.
(61) Yuan, J.; Guo, W.; Xia, Y.; Ford, M. J.; Jin, F.; Liu, D.; Zhao, H.; Inganas̈, O.; Bazan, G. C.; Ma, W. Comparing the Device Physics, Dynamics and Morphology of Polymer Solar Cells Employing Conventional PCBM and Non-fullerene Polymer Acceptor N2200. *Nano Energy* 2017, *35*, 251−262.
(62) Tvingstedt, K.; Vandewal, K.; Gadisa, A.; Zhang, F.; Manca, J.; Inganas̈, O. Electroluminescence from Charge Transfer States in Polymer Solar Cells. *J. Am. Chem. Soc.* 2009, *131*, 11819−11824.
(63) Liu, T.; Huo, L.; Chandrabose, S.; Chen, K.; Han, G.; Qi, F.; Meng, X.; Xie, D.; Ma, W.; Yi, Y.; Hodgkiss, J. M.; Liu, F.; Wang, J.; Yang, C.; Sun, Y. Optimized Fibril Network Morphology by Precise Side-Chain Engineering to Achieve High-Performance Bulk-Heterojunction Organic Solar Cells. *Adv. Mater.* 2018, *30*, 1707353.
(64) Liao, H.-C.; Tsao, C.-S.; Lin, T.-H.; Chuang, C.-M.; Chen, C.-Y.; Jeng, U.-S.; Su, C.-H.; Chen, Y.-F.; Su, W.-F. Quantitative Nanoorganized Structural Evolution for a High Efficiency Bulk Heterojunction Polymer Solar Cell. *J. Am. Chem. Soc.* 2011, *133*, 13064−13073.
(65) Liao, H.-C.; Tsao, C.-S.; Shao, Y.-T.; Chang, S.-Y.; Huang, Y.-C.; Chuang, C.-M.; Lin, T.-H.; Chen, C.-Y.; Su, C.-J.; Jeng, U.-S.; Chen, Y.-F.; Su, W.-F. Bi-hierarchical nanostructures of donor-acceptor copolymer and fullerene for high efficient bulk heterojunction solar cells. *Energy Environ. Sci.* 2013, *6*, 1938−1948.
(66) Huang, D.; Bian, F.; Zhu, D.; Bao, X.; Hong, C.; Zhou, P.; Huang, Y.; Yang, C. Ternary Solar Cells Employing Thieno[3,4-b]thiophene-Based Copolymer Offer High Performance with Large Current Density and Fine-Tuned Morphology. *J. Phys. Chem. C* 2019, *123*, 14976−14984.
(67) Huang, H.; Yang, L.; Facchetti, A.; Marks, T. J. Organic and Polymeric Semiconductors Enhanced by Noncovalent Conformational Locks. *Chem. Rev.* 2017, *117*, 10291−10318.
(68) Barker, A. J.; Chen, K.; Hodgkiss, J. M. Distance Distributions of Photogenerated Charge Pairs in Organic Photovoltaic Cells. *J. Am. Chem. Soc.* 2014, *136*, 12018−12026.
(69) Gallaher, J. K.; Prasad, S. K. K.; Uddin, M. A.; Kim, T.; Kim, J. Y.; Woo, H. Y.; Hodgkiss, J. M. Spectroscopically Tracking Charge Separation in Polymer : Fullerene Blends with a Three-phase Morphology. *Energy Environ. Sci.* 2015, *8*, 2713−2724.
(70) Marsh, R. A.; Hodgkiss, J. M.; Albert-Seifried, S.; Friend, R. H. Effect of Annealing on P3HT:PCBM Charge Transfer and Nanoscale Morphology Probed by Ultrafast Spectroscopy. *Nano Lett.* 2010, *10*, 923−930.
(71) Zhang, G.; Yang, G.; Yan, H.; Kim, J.-H.; Ade, H.; Wu, W.; Xu, X.; Duan, Y.; Peng, Q. Efficient Nonfullerene Polymer Solar Cells Enabled by a Novel Wide Bandgap Small Molecular Acceptor. *Adv. Mater.* 2017, *29*, 1606054.
(72) Wang, Q.; Wang, Y.; Zheng, W.; Shahid, B.; Qiu, M.; Wang, D.; Zhu, D.; Yang, R. Regulating Molecular Aggregations of Polymers via Ternary Copolymerization Strategy for Efficient Solar Cells. *ACS Appl. Mater. Interfaces* 2017, *9*, 32126−32134.
(73) Li, Z.; Jiang, K.; Yang, G.; Lai, J. Y.; Ma, T.; Zhao, J.; Ma, W.; Yan, H. Donor Polymer Design Enables Efficient Non-fullerene Organic Solar Cells. *Nat. Commun.* 2016, *7*, 13094.
(74) Fan, B.; Zhang, D.; Li, M.; Zhong, W.; Zeng, Z.; Ying, L.; Huang, F.; Cao, Y. Achieving over 16% Efficiency for Single-junction Organic Solar Cells. *Sci. China: Chem.* 2019, *62*, 746−752.
(75) Nikolis, V. C.; Benduhn, J.; Holzmueller, F.; Piersimoni, F.; Lau, M.; Zeika, O.; Neher, D.; Koerner, C.; Spoltore, D.; Vandewal, K. Reducing Voltage Losses in Cascade Organic Solar Cells while Maintaining High External Quantum Efficiencies. *Adv. Energy Mater.* 2017, *7*, 1700855.
(76) Shockley, W.; Queisser, H. J. Detailed Balance Limit of Efficiency of p-n Junction Solar Cells. *J. Appl. Phys.* 1961, *32*, 510−519.
(77) Yao, J.; Kirchartz, T.; Vezie, M. S.; Faist, M. A.; Gong, W.; He, Z.; Wu, H.; Troughton, J.; Watson, T.; Bryant, D.; Nelson, J. Quantifying Losses in Open-Circuit Voltage in Solution-Processable Solar Cells. *Phys. Rev. A: At., Mol., Opt. Phys.* 2015, *4*, 104020.

https://dx.doi.org/10.1021/acsami.0c01323
ACS Appl. Mater. Interfaces 2020, 12, 20393−20403